

Influence of parasitic phases on the properties of BiFeO₃ epitaxial thin films

H. Béa

Unité Mixte de Physique CNRS-Thales, Domaine de Corbeville, 91404 Orsay, France

M. Bibes

Institut d'Electronique Fondamentale, Université Paris-Sud, 91405 Orsay, France

A. Barthélémy, K. Bouzehouane, E. Jacquet, A. Khodan and J.-P. Contour

Unité Mixte de Physique CNRS-Thales, Domaine de Corbeville, 91404 Orsay, France

S. Fusil

Université d'Evry, Bâtiment des Sciences, rue du père Jarlan, 91025 Evry, France

F. Wyczisk

Thales Research and Technology, Domaine de Corbeville, 91404 Orsay, France

A. Forget, D. Lebeugle, D. Colson and M. Viret

Service de Physique de l'Etat Condensé, DSM/DRECAM/SPEC, CEA Saclay, 91191 Gif-sur-Yvette, France

Abstract

We have explored the influence of deposition pressure and temperature on the growth of BiFeO₃ thin films by pulsed laser deposition onto (001)-oriented SrTiO₃ substrates. Single-phase BiFeO₃ films are obtained in a region close to 10⁻² mbar and 580°C. In non-optimal conditions, X-ray diffraction reveals the presence of Fe oxides or of Bi₂O₃. We address the influence of these parasitic phases on the magnetic and electrical properties of the films and show that films with Fe₂O₃ systematically exhibit a ferromagnetic behaviour, while single-phase films have a low bulk-like magnetic moment. Conductive-tip atomic force microscopy mappings also indicate that Bi₂O₃ conductive outgrowths create shortcuts through the BiFeO₃ films, thus preventing their practical use as ferroelectric elements in functional heterostructures.

Materials that possess simultaneously several ferroic orders are called multiferroics [1]. Among these, magnetoelectrics are ferroelectric and ferro- or antiferromagnetic. The coupling between the two order parameters, called the magnetoelectric effect, is very interesting from the point of view of fundamental physics [2], and could also lead to applications in spintronics and other fields [3]. In order to use magnetoelectrics in devices, a preliminary step is to grow thin films of magnetoelectric materials. Among the possible candidates, BiFeO₃ (BFO) has attracted much attention [4,5,6,7]. First, it crystallises in the perovskite structure and is thus compatible with many other functional compounds. Second, it has order temperatures far beyond 300K (the ferroelectric Curie temperature is 1043K [8] and the magnetic Néel temperature 647K [9]), which is essential for applications. Third, the ferroelectric polarisation is very large, especially in thin films [7,10]. In addition, although bulk BFO is a weak ferromagnet with a magnetic moment of only $\sim 0.01 \mu_B/\text{f.u.}$ (f.u. : formula unit) [11], an increase of the magnetic moment up to about $1 \mu_B/\text{f.u.}$ in strained epitaxial films grown on STO(001) was recently reported [5]. This large moment may be related to a mixed Fe²⁺/Fe³⁺ valence [12] but questions still remain concerning the magnetic properties of BFO films. For the integration of BFO films into functional heterostructures, it is also crucial to investigate the stability of BiFeO₃, and to study the impact of possible parasitic phases on the film properties.

In this Letter, we report on the epitaxial growth of BFO films on (001) SrTiO₃ (STO) in a wide range of temperature T_{dep} (520-750°C) and oxygen pressure P (10^{-4} to 10^{-1} mbar). We find that the pure BiFeO₃ phase is formed close to $P=10^{-2}$ mbar and $T_{\text{dep}}=580^\circ\text{C}$. At lower temperature or higher pressure, Bi₂O₃ precipitates are detected while at lower pressure or higher temperature, Fe₂O₃ forms. Magnetization measurements reveal a high magnetic moment for films containing γ -Fe₂O₃ impurities while single-phase films have a low magnetic moment ($\sim 0.02 \mu_B/\text{f.u.}$) close to the bulk value. The Bi-oxide impurities have the shape of

square outgrowths with a large electrical conductivity that shortcut the insulating BFO film, as observed in conductive-tip atomic force microscopy (CTAFM) mappings.

The films have been grown by pulsed laser deposition on (001) STO substrates using a frequency tripled ($\lambda=355$ nm) Nd:YAG laser at a frequency of 2.5 Hz. In order to compensate for the high volatility of Bi and prevent Bi-deficiency inside the films, we have used a polycrystalline target with nominal composition $\text{Bi}_{1.15}\text{FeO}_3$. The sample temperature before and during the deposition process was measured by a double wavelength pyrometer pointing at the sample surface. The oxygen pressure during growth was varied from 10^{-4} to 10^{-1} mbar and, for each pressure, the growth rate ($\sim 0.4\text{-}0.6$ $\text{\AA}\cdot\text{s}^{-1}$) was estimated from X-ray reflectometry measurements.

High-resolution X-ray diffraction (XRD) spectra (using a Panalytical X'Pert PRO equipped with a Ge(220) monochromator) for some 70 nm films grown at 580°C and different pressures are shown on figure 1a. (00 l) peaks (labelled B) corresponding to the BiFeO_3 perovskite phase are visible next to the reflections of the STO substrate (labelled S). While the film grown at $6\cdot 10^{-3}$ mbar appears to be single-phase, extra peaks are detected at 10^{-4} mbar. Their positions match very well those of some intense reflections of $\gamma\text{-Fe}_2\text{O}_3$ (labelled ★), but we cannot completely exclude that these peaks may arise from Fe_3O_4 as these two materials have very similar crystal structures. At 10^{-1} mbar additional reflections corresponding to Bi_2O_3 (labelled ✦) are visible. Their positions correspond to the β phase (tetragonal) of this material, but could also be the signature of the δ phase (cubic) of Bi_2O_3 . It is possible that this parasitic phase is actually a mixture of these two very similar variants.

On figure 1b, we show three θ - 2θ scans for 70 nm films grown in a pressure of $1.2\cdot 10^{-2}$ mbar at different temperatures. The film grown at 580°C also appears to be single-phase while Bi_2O_3 peaks are detected at 520°C . At high temperature, the BFO phase does not form and instead (012)-oriented $\alpha\text{-Fe}_2\text{O}_3$ (hematite) is detected.

The results from the structural analysis of the whole films series are summarized in the pressure-temperature phase diagram of figure 2. The complexity of the diagram clearly illustrates the difficulty for optimising at the same time the Bi content integrating the film and the oxidation of Bi and Fe. As previously mentioned, no Bi-containing phase is detected at high temperature. Also, at pressures lower than $6 \cdot 10^{-3}$ mbar, $\gamma\text{-Fe}_2\text{O}_3$ forms. The diagram shows that in these two sets of conditions (low P or high T_{dep}), either a large fraction of the Bi is not oxidized and then re-evaporates due to the high vapour pressure of Bi ($\sim 10^{-3}$ mbar at 580°C) or that Bi_2O_3 , which is unstable at high temperature [13,14], decomposes into O_2 and Bi which is then easily evaporated. Alternatively, at low temperature or high pressure the excess Bi present in the target oxidises in stable Bi_2O_3 . Finally, it is only in a window close to 10^{-2} mbar and 580°C that single-phase films are obtained.

We now address the influence of the parasitic phases on the physical properties. As illustrated by figure 3, the magnetic properties of the films are extremely sensitive to the presence of $\gamma\text{-Fe}_2\text{O}_3$. Figure 3a shows a $M(H)$ hysteresis cycle recorded at 10K for a 70 nm film grown at 580°C and 10^{-4} mbar, and for which a large amount of $\gamma\text{-Fe}_2\text{O}_3$ had been detected in X-ray diffraction. A clear ferromagnetic signal is obtained, as expected since $\gamma\text{-Fe}_2\text{O}_3$ is a ferrimagnet with a saturation magnetization of $480 \text{ emu}\cdot\text{cm}^{-3}$. Even more, as the saturation magnetization for this film is about $380 \text{ emu}\cdot\text{cm}^{-3}$, assuming the ferromagnetic signal is totally due to $\gamma\text{-Fe}_2\text{O}_3$, we can deduce that $\gamma\text{-Fe}_2\text{O}_3$ represents almost 80 % of the film volume. This value is indeed consistent with the intensity of the peaks detected in X-ray diffraction (after taking account the structure factors of the diffracting lines for BFO and $\gamma\text{-Fe}_2\text{O}_3$) and with compositional Auger electron spectroscopy (AES) mappings (not shown). We must mention here that very long counting rates can be necessary to detect the presence of $\gamma\text{-Fe}_2\text{O}_3$ in very thin ($\sim 30\text{nm}$) films grown at $P \leq 2 \cdot 10^{-3}$ mbar, and showing a sizeable ferromagnetic signal.

In strong contrast with this observation is the very small magnetic moment detected for a single-phase film grown at 580°C at 6.10^{-3} mbar, see figure 3b. The magnetic properties of our single-phase films are thus consistent with those of Qi et al [15], Yun et al [16] and Eerenstein et al [17], but in strong contrast with those of Wang et al [5]. Whether it is possible to achieve large magnetic moments in single-phase films while maintaining single valence Fe^{3+} ions (for example via monoclinic distortions, as suggested by Bai et al [11]) in the BFO phase remains an open question that must be answered to define better the potential of BFO for magnetoelectric devices.

Similarly, the presence of Bi_2O_3 could also be detrimental for the use of BFO films in heterostructures. Indeed, although we were not able to find electrical data for $\beta\text{-Bi}_2\text{O}_3$, $\delta\text{-Bi}_2\text{O}_3$ is known as an excellent ionic conductor (with $\rho \approx 1 \text{ } \Omega\cdot\text{cm}$ at 1073K [18]). We have observed a film containing Bi_2O_3 with a Scanning Auger Microscope (Nanoprobe PHI680 from Physical Electronics) equipped with a SED (Secondary Electrons Detector for classical scanning electron microscopy image) and a CMA (Cylindrical Mirror Analyser for elementary Auger mapping), in order to check its chemical homogeneity. As shown in figure 4a, the surface of this film consists of low-roughness regions and of ~ 100 nm-high square outgrowths. Before recording Auger spectra on this surface, a short sputtering, required to remove atmospheric contaminants (C, O), was applied. The AES composition mapping (obtained by combining elemental mappings for Bi, Fe and O) of the same area is shown in figure 4b. It indicates that the outgrowths seen by SEM are strongly Fe-deficient and correspond to a BiO_x phase. We cannot quantify precisely the Bi/O ratio in these regions but they are likely to correspond to the Bi_2O_3 phase detected by X-ray diffraction. The regions between the outgrowths have a homogeneous (Bi, Fe, O) composition. A similar morphology, with square $\delta\text{-Bi}_2\text{O}_3$ hillocks has also been observed in $\text{Bi}_4\text{Ti}_3\text{O}_{12}$ films [19].

The influence of these Bi_2O_3 outgrowths on the electrical properties of the BFO films is exemplified in the bottom panels of figure 4. They show conductive tip AFM (CTAFM) morphology (c) and resistance (d) mappings [20] of a 70 nm thick BFO film grown on conductive Nb-doped STO, and presenting a large density of Bi_2O_3 outgrowths. The resistance map consists of a highly resistive background ($R > 6 \cdot 10^{11} \Omega$) with many low-resistance spots ($R \approx 10^7 \Omega$). Although every outgrowth does not correspond to a conductive spot, some of them clearly create shortcuts between the metallic substrate and the conductive tip that would prevent poling the BFO in ferroelectricity measurements with micron size capacitors. Some of the Bi_2O_3 outgrowths therefore nucleate directly at the substrate surface. Work is in progress to understand their evolution with film thickness. In contrast, single-phase BFO films grown on Nb-doped STO (not shown) have a homogeneous resistance level that saturates the measurements capability of our system ($R > 6 \cdot 10^{11} \Omega$).

In summary, we have grown epitaxial BFO films onto STO(001), and explored the influence of the deposition pressure and temperature on the BFO phase purity by means of X-ray diffraction. It is found that the growth of pure BFO films is strongly favoured in a window close to 580°C and 10^{-2} mbar. At lower pressure or higher temperature, the presence of Fe_2O_3 is detected while at higher pressure or lower temperature Bi_2O_3 outgrowths nucleate. The presence of these two types of impurities is detrimental to the films physical properties. Indeed, films with $\gamma\text{-Fe}_2\text{O}_3$ show an extrinsic ferromagnetic behaviour with moments up to $2 \mu_{\text{B}}/\text{f.u.}$ Resistance mappings also confirm that the presence of Bi_2O_3 is highly problematic since Bi_2O_3 outgrowths create low resistance shortcuts through the BFO film. Films for which no extra phases were detected have a low, bulk-like magnetic moment and a high resistivity.

H.B. acknowledges financial support by CNRS and the Conseil Général de l'Essone.

Figure Captions :

Fig 1. (a) X-ray diffraction spectra for three films grown at 580°C and different pressures (from bottom to top, $P=10^{-4}$ mbar, $6 \cdot 10^{-3}$ mbar and 10^{-1} mbar). (b) Spectra for three films grown at 10^{-2} mbar and different temperatures (from bottom to top $T_{\text{dep}}=520^\circ\text{C}$, 580°C and 750°C). The peaks are indexed with the following convention: B: BFO, S: STO, \star : $\gamma\text{-Fe}_2\text{O}_3$, \bullet : $\alpha\text{-Fe}_2\text{O}_3$, \blacklozenge : Bi_2O_3 .

Fig 2. Pressure-temperature phase diagram for BFO films with a nominal thickness of 70 nm.

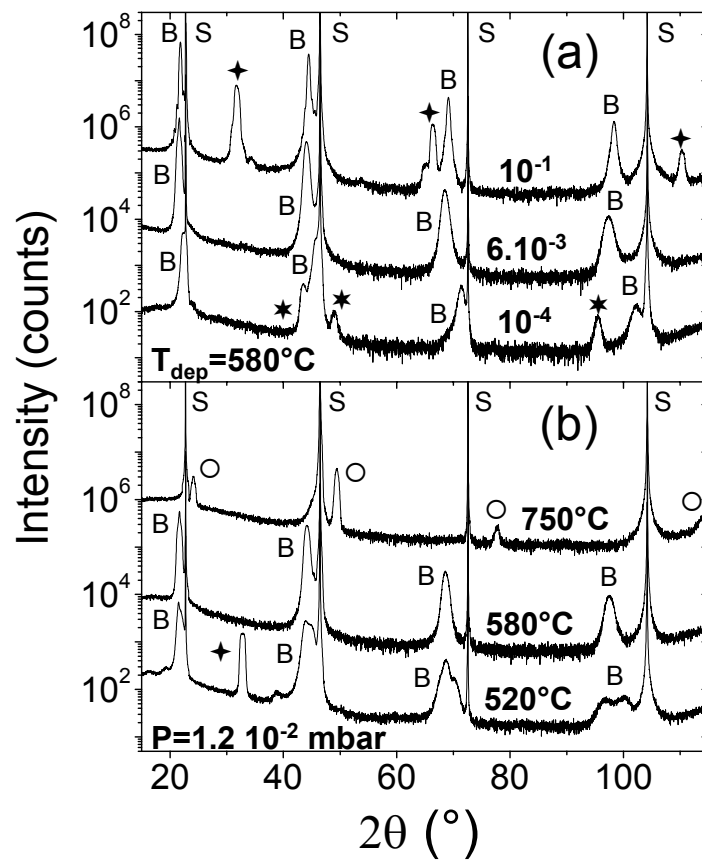
Fig 3. $M(H)$ hysteresis cycles measured at 10K with the field applied in-plane for films grown at 580°C and 10^{-4} mbar (a) and 580°C and $6 \cdot 10^{-3}$ mbar (b).

Fig 4. SEM image (a) and corresponding AES compositional mapping (b) for a BFO film containing Bi_2O_3 . (b) is a RGB image constructed by superimposing coloured element-selective mappings (red : Bi, green : Fe, blue : O). The white bar scale corresponds to 1 μm . (c) and (d) are $10 \times 10 \mu\text{m}^2$ conductive tip AFM morphology (c) and resistance (d) mappings on a similar 70 nm BFO film grown on Nb-doped STO.

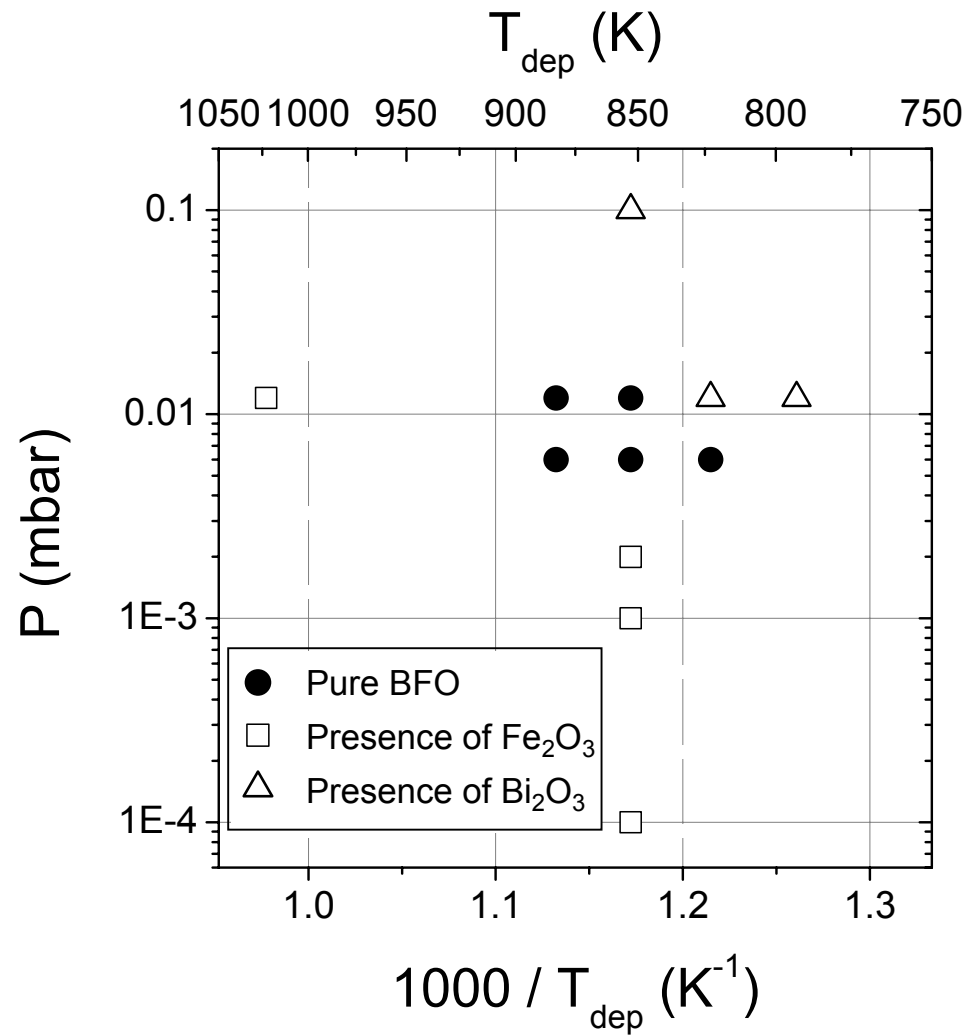
References

- [1] N.A. Hill, J. Phys. Chem. B **104**, 6694 (2000)
- [2] G.A. Smolenskii and I.E. Chupis, Sov. Phys. Usp. **25**, 475 (1983)
- [3] V.E. Wood and A.E. Austin in *Magnetoelectric Interaction Phenomena in Crystals*, Ed. A.J. Freeman and H. Schmidt (Gordon and Breach, New York, 1975)
- [4] V.R. Palkar, J. John and R. Pinto, Appl. Phys. Lett. **80**, 1628 (2002)
- [5] J. Wang et al, Science **299**, 1719 (2003)
- [6] X. Qi, M. Wei, Y. Lin, Q. Jia, D. Zhi, J. Dho, M.G. Blamire and J.L. MacManus-Driscoll, Appl. Phys. Lett. **86**, 071913 (2005)
- [7] K.Y. Yun, D. Ricinski, T. Kanashima, M. Noda and M. Okuyama, Jpn. J. Appl. Phys. **43**, L647 (2004)
- [8] G.A. Smolenskii, V.M. Yudin, E.S. Sher and Y.E. Stolypin, Sov. Phys. JETP **16**, 622 (1963)
- [9] P. Fischer, M. Polmoska, I. Sosnokowa and M. Szimansky, J. Phys. C **13**, 1931 (1980)
- [10] J. Li, J. Wang, M. Wuttig, R. Ramesh, N. Wang, B. Ruetter, A.P. Pyatakov, A.K. Zvezdin and D. Viehland, Appl. Phys. Lett. **84**, 5261 (2004)
- [11] F. Bai, J. Wang, M. Wuttig, J. Li, N. Wang, A.P. Pyatakov, A.K. Zvezdin, L.E. Cross and D. Viehland, Appl. Phys. Lett. **86**, 032511 (2005)
- [12] J. Wang et al, Science **307**, 1203b (2005)
- [13] J. Picon, J. Pharm. Chim., **10**, 481 (1929)
- [14] B. Lustman, Steel Processing, **32**, 669 (1946)
- [15] X. Qi, J. Dho, M. Blamire, Q. Jia, J.-S. Lee, S. Foltyn and J.L. MacManus-Driscoll, J. Magn. Magn. Mater. **283**, 415 (2004)

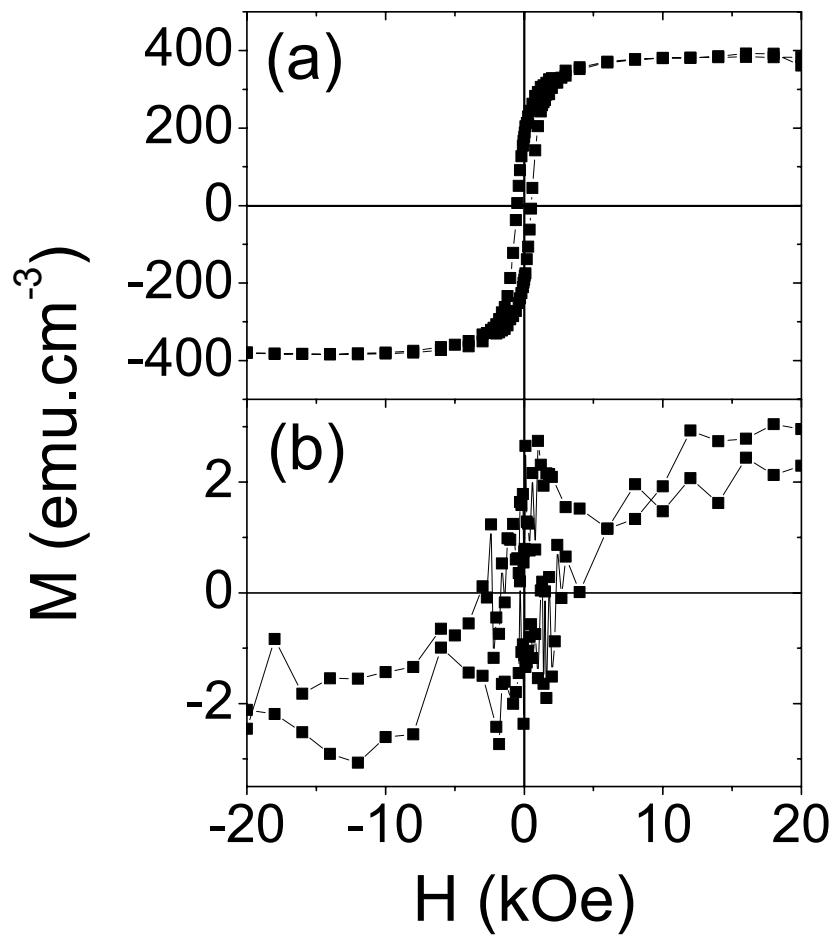
- [16] K.Y. Yun, M. Noda, M. Okuyama, H. Saeki, H. Tabata and K. Saito, *J. Appl. Phys.* **96**, 3399 (2004)
- [17] W. Eerenstein, F.D. Morrison, J. Dho, M.G. Blamire, J.F. Scott and N.D. Mathur, *Science* **307**, 1203a (2005)
- [18] T. Takahashi and H. Iwahara, *Mater. Res. Bull.* **13**, 1447 (1978)
- [19] M. Alexe, J.F. Scott, C. Curran, N.D. Zakharov, D. Hesse and A. Pignolet, *Appl. Phys. Lett.* **73**, 1592 (1998)
- [20] F. Houz , R. Meyer, O. Schneegans and L. Boyer, *Appl. Phys. Lett.* **69**, 1975 (1996)



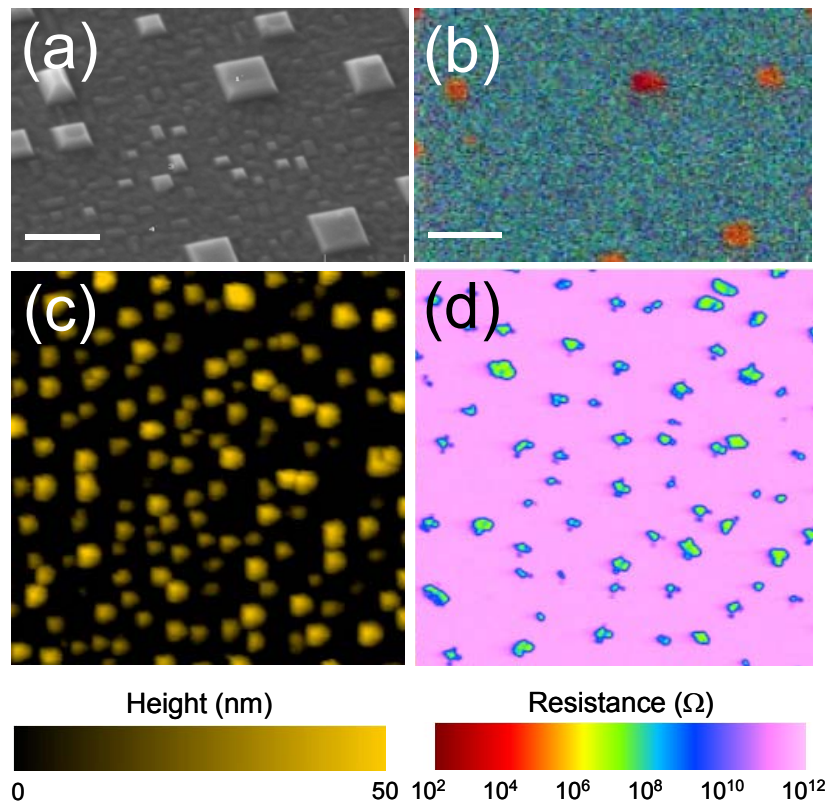
Béa et al
Fig. 1



Béa et al
Fig. 2



Béa et al
Fig. 3



Béa et al
Fig. 4